

Weak turbulence and collapses in the Majda-McLaughlin-Tabak equation: Fluxes in wavenumber and in amplitude space

Benno Rumpf ^{a,1}, Laura Biven ^{b,2}

^a*Institute of Physics, Technical University of Chemnitz
09107 Chemnitz, Germany*

^b*Max-Planck-Institute for the Physics of Complex Systems,
Nöthnitzer Straße 38, 01187 Dresden, Germany*

Abstract

The turbulent energy flow of the one-dimensional Majda-McLaughlin-Tabak equation is studied numerically. The system exhibits weak turbulence for weak driving forces, while weak turbulence coexists with strongly nonlinear intermittent collapses when the system is strongly driven. These two types of dynamics can be distinguished by their energy and particle fluxes. The weakly turbulent process can be characterized by fluxes in wavenumber space, while additional fluxes in amplitude space emerge in the intermittent process. The particle flux is directed from low amplitudes towards high amplitudes, and the energy flows in the opposite direction.

Key words: Weak turbulence; Intermittency; Wave collapse

PACS: 47.27.Eq; 05.60.+w; 47.35.+i; 52.35.-g

1 Introduction

This paper investigates two different types of turbulence, firstly, the energy transport of weakly interacting dispersive waves with low amplitudes [1], secondly, an intermittent type of turbulence [2] where localized high-amplitude structures appear from a low-amplitude background, and decay rapidly [3]

¹ Corresponding author.

E-mail address: benno.rumpf@physik.tu-chemnitz.de

² Permanent address: Bard HS Early College, 525 East Houston St., New York, NY, 10002, USA

[4][5]. Important cases of weak turbulence have been found in the dynamics of Langmuir waves in plasmas [6], capillary [7] and gravity waves [8] in hydrodynamics, in magnetohydrodynamics [9], and in Bose-Einstein condensates [10]. Collapses in Langmuir-waves [11] and self-focusing effects in optics [4],[12] are examples for the intermittent kind of behavior.

Turbulent energy flows emerge when such dynamical systems are driven on a long spatial scale, and damped on a short viscous scale [1]. Models of turbulent flows assume that the dynamics is almost Hamiltonian in the inertial range between the damping range and the driving range, and energy is transported from sources to sinks through this window of transparency with no damping or driving. Symmetries besides the time-invariance are related to conserved quantities in addition to the Hamiltonian. Examples for such quantities are the light intensity in nonlinear optics [12] or the average momenta in hydrodynamics [13]. When supplied and dissipated by driving and damping, there are fluxes also of these quantities. Fluxes that are directed from a source both toward long and toward short length scales can be modeled with an additional sink at small wavenumbers.

The fluxes of the conserved quantities determine the statistically stationary nonequilibrium of the Hamiltonian dynamics in the inertial range. The theory of weak wave turbulence computes the nonequilibrium state of weakly interacting dispersive waves, depending on boundary conditions for the fluxes. A closed kinetic equation for the two-point functions can be derived if, with the existence of a small parameter, the nonlinear coupling is much smaller than the linear dispersive effects, so that higher order correlations can be reduced to powers of the two-point function. The kinetic equations can be solved analytically. This yields the Kolmogorov-Zakharov spectrum and formulas for the fluxes [1]. The theory predicts that the system will have close to Gaussian statistics even after the weak nonlinearity is relevant. The intermittent occurrence of high-amplitude structures [14] violates the assumptions of weak turbulence, as these structures indicate strongly coherent waves. Consequently, the closure of the kinetic equation is not possible, and there is a strongly nonlinear interaction.

In recent years massive numerical experiments have been carried out [15], [16], [17], [18] to check the assumptions of the Gaussian closure of the kinetic equations. This was partly thanks to the development of dynamical system by Majda, McLaughlin, and Tabak ('MMT' equation) [15],[16], which we use in its most simple focusing version

$$i\frac{\partial\phi}{\partial t} = \left|\frac{\partial}{\partial x}\right|^{1/2}\phi - \phi|\phi|^2 + \mathcal{F} + \mathcal{D}. \quad (1)$$

ϕ is a complex field that depends on one spatial variable x . The fractional derivative $|\partial/\partial x|^{1/2}\phi$ stands for the Fourier-transform of the term $\sqrt{|k|}a_k$ with the mode $a_k = (1/L) \int \phi(x) \exp(ikx)dx$, or equivalently, for the inverse of

a fractional integral [19]. The concave dispersion $\omega(k) = \sqrt{|k|}$ yields more four wave resonances than a convex dispersion law (such as the dispersion $\omega(k) \sim k^2$ of the nonlinear Schrödinger equation) does. This leads to an efficient energy transport even in only one dimension, and allows numerical simulations in a wider range in the wavenumber space compared to simulations in two or three spatial dimensions. The general MMT equation has fractional derivatives of any order both in the linear and in the nonlinear part, but the semiderivative and the simple nonlinearity of (1) is by the signs of the fluxes [17] suitable for the study of wave turbulence.

\mathcal{D} is a damping term that affects very short waves and very long waves only. The driving force \mathcal{F} affects waves on an intermediate length scale. The length scale of the driving force and the length scale of the short-wave damping are widely separated by the window of transparency where no damping or driving occurs.

The MMT equation for zero driving \mathcal{F} and damping \mathcal{D} derives from the Hamiltonian (or "energy") $E = E_2 + E_4$, with the quadratic coupling part $E_2 = \int |\partial/\partial x|^{1/4} \phi|^2 dx = \sum \sqrt{k} |a_k|^2$, and the nonlinear part $E_4 = - \int |\phi|^4 / 2 dx$. The wave action or "particle number" $n = \int |\phi|^2 dx = \sum |a_k|^2$ is a second conserved quantity which is related to the system's phase symmetry.

Numerical simulations of (1) found the Kolmogorov-Zakharov spectrum as predicted by weak turbulence theory, but also concluded that most of the energy transport is related to strongly nonlinear collapses [17], which coexist with weakly interacting low-amplitude waves. In this case, high-amplitude peaks emerge in a very similar way as in the corresponding Hamiltonian systems where this process maximizes the entropy [20]. Pure wave turbulence for the MMT equation has been found for freely decaying turbulence [16], but not in the stationary nonequilibrium. A steeper spectrum than predicted by wave turbulence has been obtained for the defocusing MMT equation (where the sign of the nonlinearity is opposite to the focusing equation (1)) and in some cases for the focusing equation [16]. This lead to the proposal of an alternative closure from which the steeper spectrum can be derived [15].

The aim of this paper is to study both the weakly turbulent state and the collapse dynamics by measuring the fluxes of energy and particles. In fact, as we show here, flux measurements are a more reliable indicator of the transport dynamics than the energy spectrum. We compute energy and particle fluxes by measuring the input and output of these quantities that is caused by the driving force and the damping in our numerical experiments.

We give evidence that a pure weakly turbulent process emerges if the driving forces are sufficiently weak. The fluxes in wavenumber space correspond to the predictions of weak turbulence theory (section 3).

For stronger external driving we find a transition to a process where weak turbulence and collapse dynamics coexist. Despite the fact that the formation of high-amplitude structures is not in agreement with the assumptions of weak turbulence our simulations of (1) find the weak turbulence spectrum.

The collapse dynamics is characterized by fluxes of energy and particles both in wavenumber and in amplitude space. These fluxes in amplitude space contain information on the coherent process (section 4).

We present numerical results for one simulation that is representative for weak driving and damping (Figs. 2,3,4) and one for strong driving and damping (Figs. 2,6,7,8). Figs. 9,10 show data from another simulation with a medium power driving force. These two figures show time-dependent quantities, all other figures show time-averaged quantities. Figs. 5,11 show results of a series of simulations with various driving forces.

2 Numerical method

We integrate equation (1) numerically using a pseudospectral method with an integrating factor similar to the method described in [15]. $\phi(x)$ is defined on the interval $[0, 4096]$ with periodic boundary conditions. For its integration we use $L = 4096$ modes, with wavenumbers k in the Brillouin zone $]-\pi, \pi]$. The linear part can be eliminated analytically using an integrating factor, and the resulting non-stiff equation is integrated with a multistep (Adams) method.

We use driving and damping forces that act as time-periodic δ -kicks, while the system is governed by the Hamiltonian MMT equation for one time unit between the subsequent kicks. The external driving force \mathcal{F} is applied to the modes in the interval $20 < |k|L/(2\pi) \leq 40$. The driving δ -kicks increase the amplitude as $a_k \rightarrow (1 + \lambda)a_k$ with $\lambda = 0.1$. This driving force is only applied to modes with an amplitude below a threshold $|a_k|^2 < c_0/k$, so that the total energy input reduces when more modes exceed this threshold.

The damping \mathcal{D} is applied both at low wavenumbers ($|k|L/(2\pi) \leq 20$) and at high wavenumbers $\pi/2 \leq |k|$, while modes in the window of transparency $40 < |k|L/(2\pi) < L/4$ are neither damped and nor driven. The broad high- k damping minimizes the aliasing error of the numerical computation. Ideally, the low- k damping and driving range should also be chosen larger, but this would narrow the window of transparency. The damping δ -kicks decrease the amplitude as $a_k \rightarrow (1 - \lambda)a_k$ with $\lambda = 0.1$. This damping is applied only to modes in the high- k window when the amplitude exceeds the threshold $|a_k|^2 > c_+/|k|$, and to low- k modes above the level $|a_k|^2 > c_-$. This type of damping becomes more effective when more modes exceed this threshold.

The purpose of this type of damping and driving is purely practical: Damping and driving by time-periodic δ -kicks has the advantage that the input and output of energy and particles can be measured directly, and are distinguishable from the Hamiltonian dynamics of (1). The effect of the kicks is quite small in all our simulations, so that there is little difference between snapshots before and after the kicks. The damping is restricted to the two windows in k -space in order to keep the window of transparency free of dissipation. The threshold

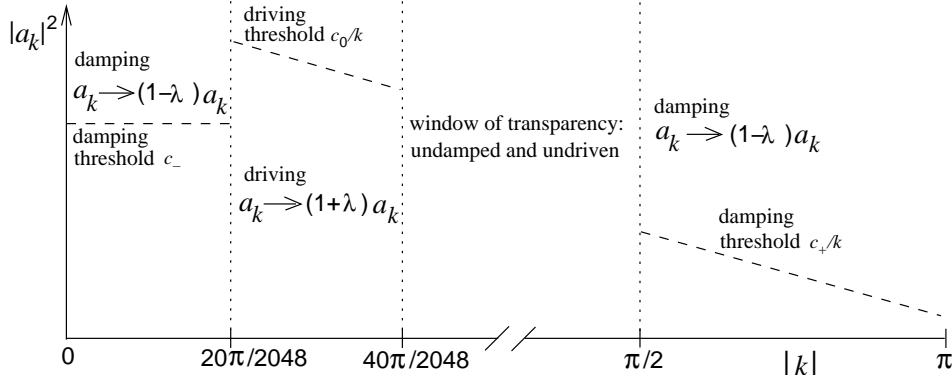


Fig. 1. The driving force acts on modes a_k with $20 < |k|L/2\pi \leq 40$ when $|a_k|^2$ is below a threshold c_0/k . The driving δ -kicks increase these modes as $a_k \rightarrow (1 + \lambda)a_k$ with $\lambda = 0.1$. The damping decreases the modes of the interval $|k|L/2\pi \leq 20$ as $a_k \rightarrow (1 - \lambda)a_k$ when $|a_k|^2$ above a constant threshold c_- , as well as the modes in the interval $\pi/2 < |k| \leq \pi$ when $|a_k|^2$ is above a threshold c_+/k .

parameters c_- , c_0 and c_+ allow us to control the amplitudes in the driving and the damping regions. In particular, the driving force can be increased by increasing the threshold c_0 . This type of forcing is similar to coupling the system to heat baths with different temperatures in the driving and damping regions. It appears that this leads to a relatively quick relaxation to a statistically stationary state. In this state, it is equivalent to other types of forcing that cause the same fluxes. In our simulations we choose $c_- = c_0/60$ and c_0 slightly larger than c_+ . This choice has turned out to yield Kolmogorov-Zakharov spectra with relatively small deviations at the boundaries of the window of transparency.

For comparison, we have performed simulations with time-continuous driving and hyperviscous damping, which show no significant differences to the δ -driven case. Our results are also in agreement with those reported in the literature. In particular, we have found WT spectra [17] for the focusing MMT equation (1), while we find the steeper MMT spectrum [15] for its defocusing version. The results in this paper are robust under various modifications of the scheme. We have performed simulations with various resolutions from 1024 modes to 8192 modes, and various types of damping and driving. Other modifications include the ranges in k -space where damping and driving is applied, the time intervals between the kicks and the strength of the kicks. We have tested of the integration scheme for undamped and undriven equations by simulating the well-known solitons of the nonlinear Schrödinger equation, and by checking the conservation of energy and particles by the MMT equation.

In all simulations the system is first allowed to relax until it reaches an almost stationary nonequilibrium state, which takes $10^4 - 10^5$ time units depending on the particle input. Time-averaged quantities such as power spectra and energy fluxes are computed for the nonequilibrium state in a second round of integration. In this state, the input of particles and energy matches the

output, and the energies E_2 and E_4 and particle number n are constant with only small fluctuations. The integration time is long enough to average away the effect of these random fluctuations.

3 The weakly turbulent state

3.1 Power spectrum and amplitude statistics

The dynamics of (1) depends critically on the strength of the driving force and the damping, and we study the dynamics in two representative simulations, one for weak driving, and one for strong driving. Fig.2(a) shows the time-averaged wave action $n_k = \langle |a_k|^2 + |a_{-k}|^2 \rangle$ over the wavenumber. Both for the weakly and the strongly driven system, we obtain a Kolmogorov-Zakharov spectrum $n_k = c/(kL/2\pi)$ in the window of transparency. The coefficient c measures the particle number for waves in the window of transparency, which is $c = 2.4$ for the weakly driven system and $c = 27$ for the strongly driven system. In the regions in k -space where the driving (damping) is applied, n_k is higher (lower) than the level of the spectrum $n_k = c/(kL/2\pi)$. In the weakly

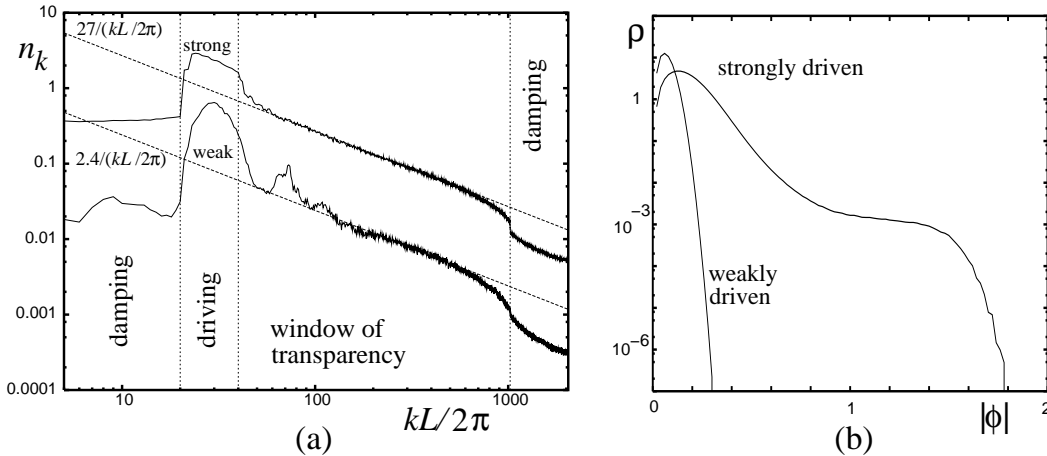


Fig. 2. (a): The time-averaged wave-action $n_k = \langle |a_k|^2 + |a_{-k}|^2 \rangle$ ($n = \sum n_k$ is the total particle number) of the MMT equation exhibits Kolmogorov-Zakharov spectra $n_k \sim k^{-1}$ in the window of transparency both for weak and for strong driving forces. The dotted lines are fits $n_k = c/(kL/2\pi)$ with $c = 2.4$ and $c = 27$ of the spectra in the window of transparency. (b): Probability density of the amplitude $|\phi|$ for the weakly and the strongly driven system. The probability for high amplitudes decays as $\sim \exp(-|\phi|^2)$ for the weakly driven system. The shoulder-shaped distribution for the strongly driven system exhibits a significant probability for high-amplitude structures ($|\phi| \approx 1.5$). Particle number and energy fluctuate about constant values in both simulations (weak driving: $n \approx 18$, $E_2 \approx 7.5$, $E_4 \approx -0.08$, strong driving: $n \approx 150$, $E_2 \approx 75$, $E_4 \approx -10$).

driven system, the spectrum has also two humps at harmonics of the driving force at the low- k end of the window of transparency. These effects could be reduced with a driving force that acts on a broader k -band.

In Fig.2(b), $\rho(|\phi|)d|\phi|$ gives the probability that the amplitude at one location is between $|\phi|$ and $|\phi| + d|\phi|$. The distribution of the amplitudes is qualitatively different for the two simulations. In the weakly driven system we find a distribution $\rho \sim |\phi|exp(-|\phi|^2)$ without any incident of an amplitude $|\phi| > 0.3$ during $5 \cdot 10^5$ integration cycles. The probability density of the strongly driven system is again gathered at small $|\phi|$, but its shoulder-like shape shows that amplitudes of the order of one are obtained with a probability of about 10^{-3} .

3.2 Input and output of particles and energy

Fig.3 shows the input and output rates of particles and energy by the driving and damping forces as functions of k for the simulation with weak driving of Fig.2. For clarity, low wavenumbers (a) and high wavenumbers (b) are plotted on different scales. Positive Δn_k show the input of particles in the driving range (Fig.3(a)), while negative Δn_k indicate particle losses both in the low- k (Fig.3(a)) and in the high- k damping ranges (Fig.3(b)). The total particle number is unchanged since input and output of particles match as $\sum \Delta n_k \Delta k = 0$, and the particle number is also conserved by the Hamiltonian dynamics.

A change Δn_k of the particle density at the mode k also changes the density of the coupling energy E_2 at this wavenumber by $\omega(k)\Delta n_k \Delta k$. Consequently, the gains and losses of particles by the driving and damping translate to gains and losses of energy via the coefficient $\omega(k) = \sqrt{k}$. The energy gain in the

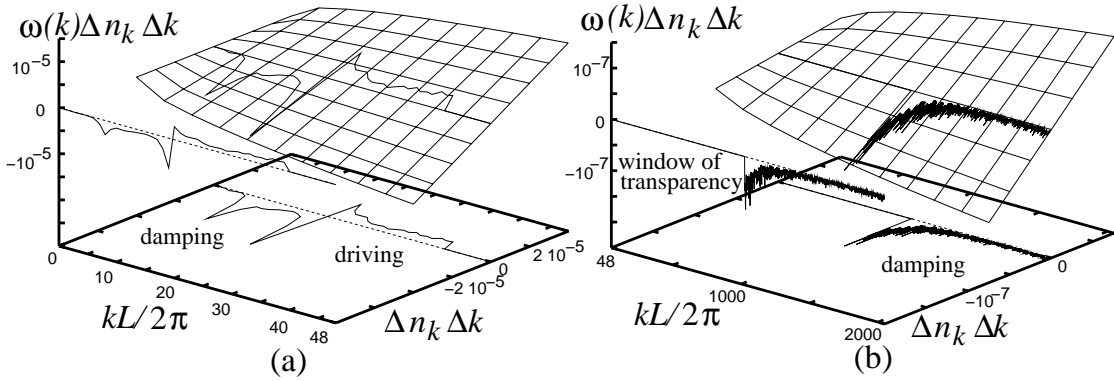


Fig. 3. Particle- and energy-balance for the weakly driven system of Fig.2. The driving and damping forces change the particle contents of the mode k by $\Delta n_k \Delta k$ per time unit. Δn_k is the change of the particle density, $\Delta k = 2\pi/4096$ is the distance between adjacent modes. This particle input or output is connected to a change of the coupling energy by $\omega(k)\Delta n_k \Delta k$. (a): The low- k damping range and driving range. (b): The window of transparency and the high- k damping range.

driving range matches the energy loss in the two damping ranges, so that $\sum \omega(k) \Delta n_k \Delta k = 0$. The influence of driving and damping on the nonlinear energy E_4 is very small.

3.3 Particle flux of the weakly driven system

In a statistically stationary nonequilibrium state, the particle number $|a_k|^2 + |a_{-k}|^2$ at $|k|$ fluctuates about a time-independent average value n_k (Fig.2a). Particles that are injected in the driving range flow to the two damping regions, where particles are removed at the same rate. This defines two fluxes of particles, one in a direct cascade through the window of transparency (where no particles are injected or removed) to the high- k damping, and one in an inverse cascade to the low- k damping range. The particle flux $q(k)$ through k -space follows from the continuity equation for the particles

$$\Delta q(k)/\Delta k - \Delta n_k/\Delta t = 0 \quad (2)$$

where $\Delta k = 2\pi/4096$ and $\Delta t = 1$ in our simulations (a corresponding partial differential equation $\Delta \rightarrow \partial$ applies to continuously damped and driven, infinite systems). Δn_k is the particle input or output by the external driving and damping, which is minus the particle change that is caused by the flux

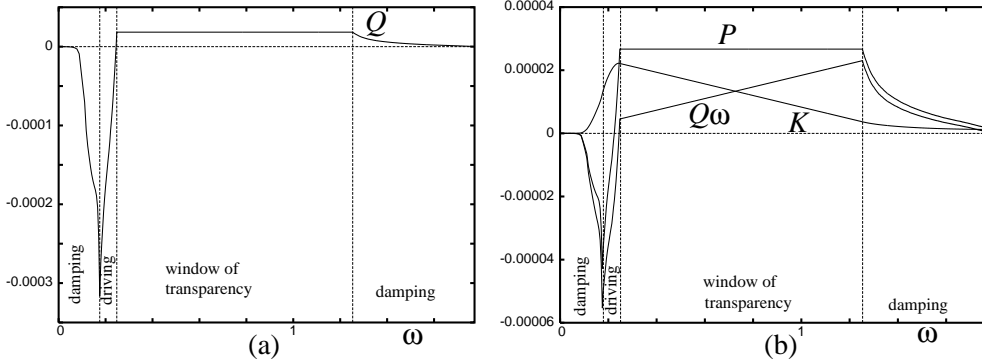


Fig. 4. Particle- and energy-fluxes in ω -space for the weakly driven system of Fig.2. (a): The particle flux Q is positive (i.e. particles move toward high ω) in the window of transparency and in the high- ω (or high- k) damping range, and it is strongly negative in the low- ω damping range and in most of the driving range. Its gradient is negative in the damping ranges, where particles are removed from the system, and positive in the driving range, where particles are injected into the system. Q is constant in the window of transparency. It is zero at $\omega = 0$ and at $\omega = \sqrt{\pi}$, as the particle input matches the particle output. (b): The energy flux P has the same qualitative characteristics as Q . $Q\omega$ is the energy drift of the particle flux. $K = P - Q\omega$ is the energy transfer from the inverse cascade at low ω (where energy is released) to the direct cascade where energy is absorbed by the energy drift.

$q(k)$. This definition yields the minus sign in equation (2). The particle flux is obtained as $q(k) = \sum_{\tilde{k}=0}^k \Delta n_{\tilde{k}} \Delta \tilde{k} / \Delta t$. As the system's particle number is constant, the particle flux vanishes at $k = 0$ and at the short-wave boundary of the Brillouin-zone $k = \pi$. The flux can be defined in frequency space as $Q(\omega) = q(k(\omega))$ which has similar properties since $\omega(k) = \sqrt{|k|}$ is bijective in the interval $[0, \pi]$. Fig.4 shows the particle flux $Q(\omega)$ for the simulation of Fig.3. A negative sign indicates a flux toward small frequencies (or wavenumbers), a positive sign shows a flux to high ω . The flux is strongly negative in the the inverse cascade at low ω . The sign changes at some point in the driving region, and in the window of transparency there is a small positive flux to high ω . The slope is positive in the driving range, and negative in the damping ranges. The flux of this direct cascade is k -independent in the window of transparency, and decays in the damping region at $k > \pi/2$ where particles are absorbed.

3.4 Energy flux in the weakly driven system

Similarly to the particles, the energy that is injected at the driving scale flows to the two damping ranges. The energy flux $p(k) = \sum_{\tilde{k}=0}^k \omega(\tilde{k}) \Delta n_{\tilde{k}} \Delta \tilde{k} / \Delta t$ can be defined from the energy continuity equation

$$\Delta p(k) / \Delta k - \omega(k) \Delta n_k / \Delta t = 0 \quad (3)$$

where the energy sources and sinks are located at the same wavenumbers as the particles sources. The constant energy of the nonequilibrium state requires that there is no flux through the boundaries $p(0) = p(\pi) = 0$. Fig.4(b) shows the corresponding flux in ω -space $P(\omega) = p(k(\omega))$.

As particles move toward higher values of ω in the direct cascade, their load with coupling energy increases proportionally to ω . The energy transport of the particle flux is measured by the quantity $Q(\omega)\omega$, which we call the energy drift. The energy drift depends on ω even in regions that are remote from energy sources and sinks: In the window of transparency, it increases with ω while the energy flux $P(\omega)$ and the particle flux $Q(\omega)$ are constant. The inverse cascade is linked to a negative energy drift that approaches zero for $\omega \rightarrow 0$.

$K = P - Q\omega$ amounts for the discrepancy of the energy flux and the energy drift. It measures the part of the energy flux P that is not related to the particle flux. We call K the energy transfer term, because it describes the transfer of energy from the inverse cascade to the direct cascade: Particles of the inverse cascade release energy as they move towards lower ω , which feeds the energy transfer process. The energy transfer K shifts this energy toward higher frequencies by four-wave interactions. This energy is absorbed

by the energy drift in the direct cascade, where the particles demand energy in order to move to higher ω . In other words, the inverse cascade drives the direct cascade via the energy transfer. K is positive for all wavenumbers in this simulation, and vanishes at the boundaries.

Fig.4 and Fig.2 give evidence for a pure weakly turbulent flow without strongly nonlinear processes. The amplitudes are always small, and the coupling part of the Hamiltonian carries almost all energy. The nonlinearity acts only as a weak coupling force of linear waves, without directly interfering in the energy input or output. As suggested in [17], the main ingredient to obtain such a solution numerically is a sufficient number of modes in the low- k damping range and in the driving range. This avoids a bottleneck in the particle flow of the inverse cascade due to the lack of resonant modes.

The Zakharov solution $n_k \sim 1/k$ to the kinetic equation involves a finite energy flux $P > 0$ and a zero particle flux $Q = 0$ in the direct cascade. This may be regarded as the limit of the fluxes of Fig.4 for an infinite extension of the window of transparency, with a high-frequency damping at $\omega \rightarrow \infty$. The energy transfer K is again fed by the release of energy in the inverse cascade, but it is qualitatively different in the direct cascade. The Zakharov solution has a zero energy drift in the direct cascade, so that the energy transfer equals the energy flux $K = P$, and is ω -independent in the window of transparency.

3.5 Transition of the particle flux

We now determine how the strength of the particle flux changes with the particle number. We run a number of simulations with various driving powers and determine the coefficient c of the spectrum $n_k = c/(kL/2\pi)$ for each of these simulations. $c = 2.4$ of Figs.3,4 corresponds to the weakest driving force. Fig.5 shows the strength of the particle fluxes Q of the direct cascade and the inverse cascade for various driving forces. Q_+ is the particle flux in the window of transparency, where the particle flux of the direct cascade reaches its maximum. $|Q_-|$ is the modulus of the particle flux at the boundary between the low- k damping range and the driving range (see Figs.3(a),4(a)). Both fluxes increase with c , and the lines in Fig.5(a) are tentative interpolations $Q \sim c^{3.45}$. For comparison, the wave turbulence closure gives $Q \sim c^3$ for four-wave interactions.

The input of particles and of energy matches the output only for a certain ratio [1] of the strengths of the fluxes Q_+ and Q_- . We assume for simplicity that the driving force acts only at one effective frequency ω_0 , and that the high- and low-frequency damping act at ω_+ and ω_- respectively. The particle output rates at these sinks are Q_+ and $|Q_-|$, with corresponding energy output rates $Q_+\omega_+$ and $|Q_-|\omega_-$. Input of particles $Q_+ + |Q_-|$ and of energy $(Q_+ + |Q_-|)\omega_0$ and their output match if $Q_+/|Q_-| = (\omega_0 - \omega_-)/(\omega_+ - \omega_0) \approx 0.05$, where we have set $\omega_+ \approx 1.5$, $\omega_- \approx 0.15$, $\omega_0 \approx 0.21$. Fig.5(b) shows this ratio of the

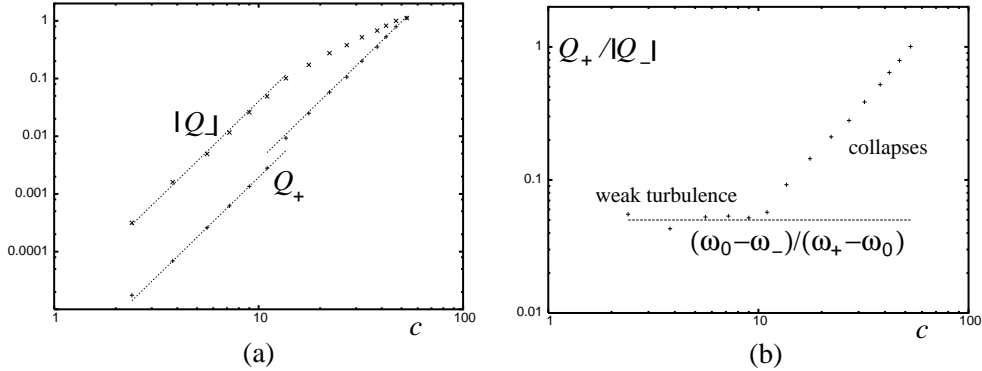


Fig. 5. (a): Maximum particle flux of the direct cascade Q_+ and of the inverse cascade $|Q_-|$ versus the coefficient c of the wave action $n_k = c/(kL/2\pi)$. The lines give a fit with $\sim c^{3.45}$. (b): Ratio of direct and inverse cascade versus the wave action. For low particle densities, the ratio agrees to the prediction of weak turbulence theory $Q_+/|Q_-| = (\omega_0 - \omega_-)/(\omega_+ - \omega_0) \approx 0.05$, where $\omega_+ \approx 1.5$ is the average frequency of high- k damping and $\omega_- \approx 0.15$ of low- k damping, while $\omega_0 \approx 0.21$ is the frequency where the driving occurs.

two fluxes. For weak driving forces (corresponding to $c < 10$), Q_+ and $|Q_-|$ both increase at the same rate with c , so that we find the expected fixed ratio of fluxes $Q_+/|Q_-| \approx 0.05$ (line in Fig.5(b)). Above $c \approx 10$ however, the flux $|Q_-|$ increases at a lower rate with c , and the ratio $Q_+/|Q_-|$ increases. This is obviously not compatible with the assumption of a weakly turbulent state.

4 Collapses and fluxes in amplitude space

4.1 Particle flux and energy flux for the strongly driven system

Above the transition point of Fig.5(b) we observe intermittent high-amplitude structures. These structures are visible in the amplitude statistics of Fig.2(b), but not in the power spectrum Fig.2(a) since only few of the particles contribute to collapses, and their Phillips spectrum decays more rapidly with k than the WT spectrum of the low-amplitude background [18]. We focus on the fluxes of particles and energy related to the strongly nonlinear events, and mention their dynamical properties only briefly.

Figs.6-8 show results for the strongly driven system of Fig.2 with $c = 27$. Fig.6 shows the fluxes of particles and energy in wavenumber space. Again as in Fig.3(a), the particle flux in Fig.6(a) is negative at small ω and positive above the driving range, and it reaches zero both for high and for low ω . Compared to the weakly driven system of Fig.3, the particle fluxes are stronger by three orders of magnitude, and a higher share of particles (one fourth compared to one twentieth) moves toward high ω . The relative strength of the

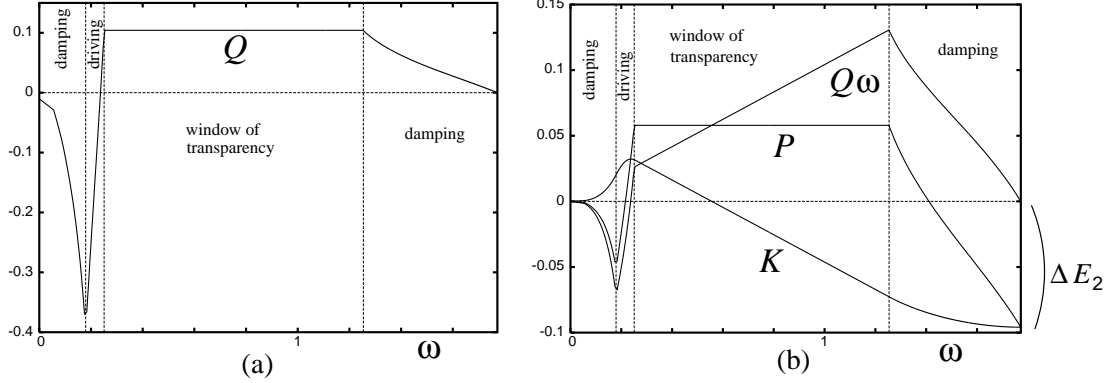


Fig. 6. Particle- and energy-fluxes of the strongly driven system of Fig.2. (a): The particle flux Q has the same shape as for the weakly driven system (Fig.3), but the positive flux towards high ω has a higher relative strength. Again there is no net gain or loss of particles. (b): Unlike for the weakly driven system (Fig.3b), the energy flux P and the energy transfer K become negative for high ω .

direct cascade leads to a significant change of the energy fluxes in Fig.6(b): The dissipation at high ω causes to a decay of the energy flux P below zero. The dissipation of coupling energy exceeds its input by ΔE_2 within each cycle of driving and damping. Contrary to this apparent loss of coupling energy, E_2 is constant with only small fluctuations, and consequently there must be an additional source of coupling energy to compensate this loss.

This source also plays a role for the energy transfer K . K is positive in the lower part of the window of transparency, which indicates an energy transfer from the inverse cascade that is feeding the energy drift in the direct cascade. However, the sign of K changes within the window of transparency, and $K < 0$ suggests that energy is transferred from a source at high ω to lower frequencies, where it feeds the energy drift $Q\omega$. The energy drift is therefore now driven both by the energy transfer from the inverse cascade, and from a transfer of energy from some other source in the high- ω dissipation range. We will now study this source of energy.

4.2 Nonlinear energy

Fig.7 shows the average input and output of particles and of nonlinear energy E_4 as a function of the amplitude $|\phi|$. For a formal definition, we define the ceiling function

$$c(v, w) = \begin{cases} v & \text{for } v < w \\ w & \text{for } v \geq w \end{cases}$$

for real v, w . The square norm of the ceiling function of the amplitude $|\tilde{\phi}(x)|$ is an amplitude-dependent particle number $n(|\phi|) = \int c^2(|\tilde{\phi}(x)|, |\phi|) dx$. This particle number is obtained when the amplitude is set to equal $|\phi|$ at all locations where it exceeds $|\phi|$. The derivative $n_{|\phi|} = \partial n(|\phi|)/\partial |\phi|$ gives the nonnegative density of particles as a function of the amplitude $|\phi|$, and $n = \int_0^\infty n_{|\phi|} d|\phi|$ is the total particle number. $\Delta n_{|\phi|}$ as shown in Fig.7(a),(b) is the time-averaged difference of $n_{|\phi|}$ before and after the driving and damping kick. In other words, $n_{|\phi|}$ is the particle density in amplitude space that is injected or removed by the driving and damping. There is a net particle input at low amplitudes and a net particle output at high amplitudes. The area under the curve where particles are gained equals the area under the curve where particles are removed, as there is no net gain or loss of particles.

Analogously to the particle density, a density of nonlinear energy in amplitude space $E_{4|\phi|} = \partial E_4(|\phi|)/\partial (|\phi|)$ derives from the amplitude-dependent energy $E_4(|\phi|) = -\int c^4(|\tilde{\phi}(x)|, |\phi|)/2 dx$. $\Delta E_{4|\phi|}$ of Fig.7(a),(c) is the average difference of $E_{4|\phi|}$ before and after the driving and damping. This shows a net gain of nonlinear energy at high $|\phi|$ where particles are dissipated, and a small net energy loss at low $|\phi|$ where particles are injected. As the change of the amplitude $\Delta|\phi| \ll |\phi|$ is small compared to the amplitude, the change

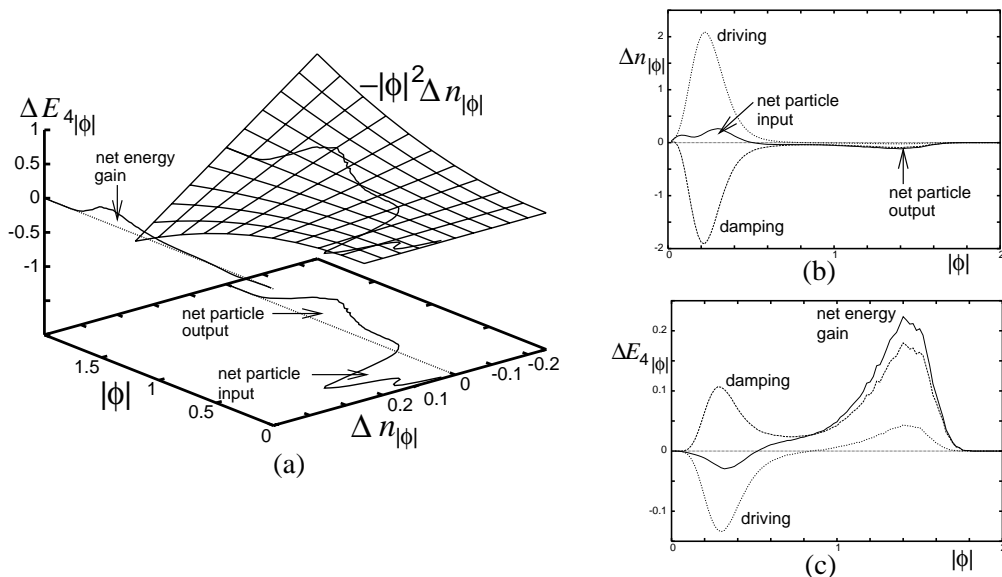


Fig. 7. Balance of particles n and nonlinear energy E_4 as a function of the amplitude for the strongly driven system of Fig.2. (a): Damping and driving lead to a net particle gain at those locations in real space where the amplitude is small ($|\phi| \approx 0.3$) and to a net particle loss at higher amplitudes ($|\phi| \approx 1.4$). The net losses match the net gains. The losses at high $|\phi|$ lead to a gain of nonlinear energy $-\Delta E_{4|\phi|}$. (b): Driving and damping inject and remove particles mainly at low $|\phi|$. The net particle change (see also (a)) is the sum of the driving and the damping process. (c): The net change of the energy E_4 (see also (a)) as the sum of the driving and the damping process.

of the energy density is connected to the change of the particle density by $\Delta E_{4|\phi} \approx -|\phi|^2 \Delta n_{|\phi}$. Sources and sinks of the particles translate to sinks and sources of nonlinear energy via the factor $-|\phi|^2$. This is somewhat similar to the correspondence between sources of particles and coupling energy in k -space of Fig.3, where the coefficient is $\omega(k)$. The particle sink at high $|\phi|$ becomes a substantial source of energy E_4 , as the factor $-|\phi|^2$ is quite significant there. At the same time, the particle source at low $|\phi|$ is only a small energy sink. Figs.7 (b) and (c) distinguish between the effects of driving, damping, and the net effect of the superposition of both (as in (a)). Fig.7 (b) shows that that most particles are both injected and dissipated at locations where the amplitude is small. The sum of both curves shows again the net particle input at $|\phi| \approx 0.3$ and the output at $|\phi| \approx 1.4$. Fig.7(c) shows the corresponding changes of nonlinear energy, where the gain at high amplitudes is the most important effect. In contrast to this, no relevant change of the nonlinear energy is observed in the simulation with weak driving of Fig.3. In this case, the particles are both injected and removed at low amplitudes, and there is no particle dissipation and no energy gain at high $|\phi|$.

4.3 Fluxes in amplitude space and energy from collapses

The particle source at low $|\phi|$ and the sink at high $|\phi|$ induce a particle flux $\Lambda(|\phi|)$ through amplitude space. Fig.8(a) shows this particle flux, which is obtained from $\partial\Lambda(|\phi|)/\partial|\phi| - \Delta n_{|\phi}/\Delta t = 0$ by integration of $\Delta n_{|\phi}$ over $|\phi|$. Similarly to the particle fluxes Q in ω -space (Figs.3(a),4(a)), it is zero both for low and for high $|\phi|$, as the total particle number is constant. $\Lambda(|\phi|)$ is positive, which shows that the particle flux is directed from low amplitudes to high amplitudes. Unlike the fluxes in k or ω -space, the sources and sinks overlap, so that only a part of the total particle input contributes to the flux, while most particles are again removed by the damping at the same $|\phi|$.

A nonlinear energy "flux" $M(|\phi|)$ is obtained by integrating $\partial M(|\phi|)/\partial|\phi| - \Delta E_{4|\phi}/\Delta t = 0$. This quantity is negative at small amplitudes, since the particle sources at low $|\phi|$ are sinks of E_4 . At higher $|\phi|$ it increases with the amplitude, since the particle sinks in this domain are powerful sources of E_4 . It reaches a saturation value ΔE_4 at $|\phi| \approx 1.8$, which is the net gain of nonlinear energy by the driving and the damping.

In a similar way, a "flux" $\Pi(|\phi|)$ of coupling energy in amplitude space can be defined. The coupling energy of the locations x where the amplitude $\tilde{\phi}(x)$ is below the threshold $|\tilde{\phi}(x)| \leq |\phi|$ is $E_2(|\phi|) = \int u(|\phi| - |\tilde{\phi}(x)|) |\partial/\partial x|^{1/4} \tilde{\phi}(x)|^2 dx$, where $u(l \geq 0) = 1, u(l < 0) = 0$ is the unit step function. The corresponding energy density in amplitude space is $E_{2|\phi} = \partial E_2(|\phi|)/\partial|\phi|$. We measure the time-averaged energy input or output $\Delta E_{2|\phi}$ of the density of the coupling energy in amplitude space. $\Pi(|\phi|)$ is obtained by integrating $\Delta E_{2|\phi}$ over $|\phi|$ (Fig.8(d)). $\Pi(|\phi|)$ is zero at $|\phi| = 0$, and decreases to a constant value $\Delta E_2 < 0$

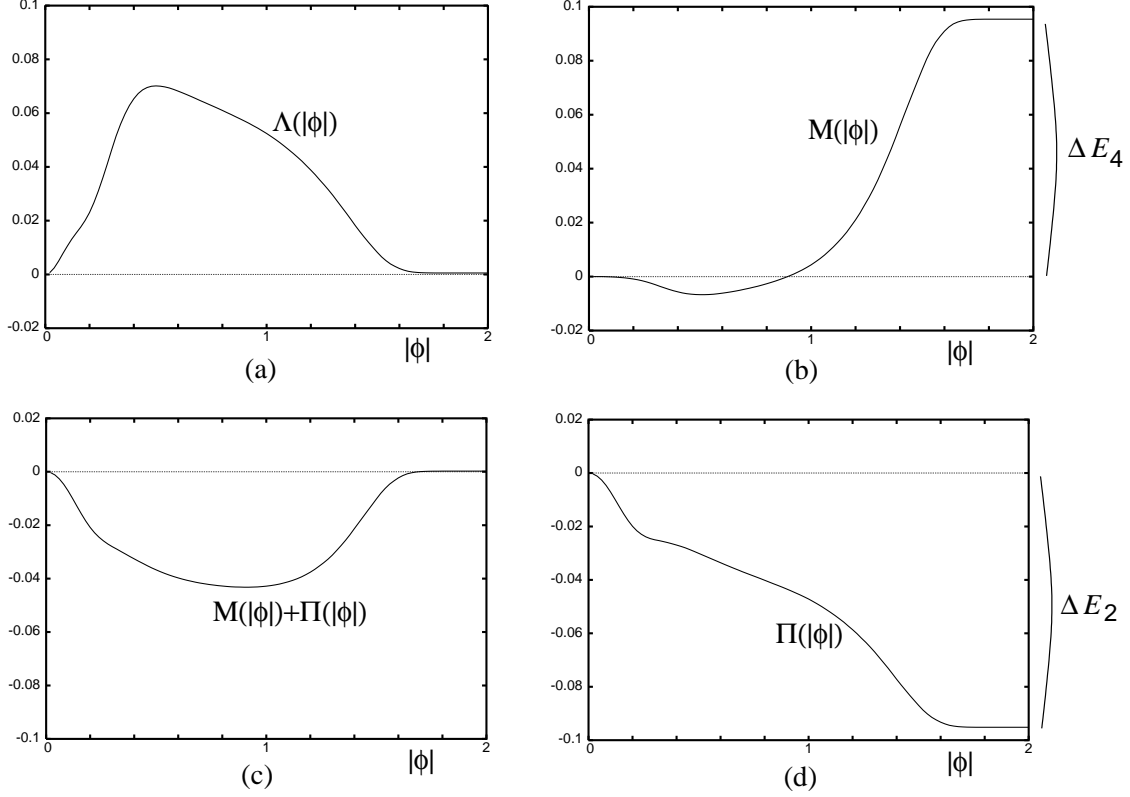


Fig. 8. Particle and energy fluxes in amplitude ($|\phi|$) space. (a) Particle flux $\Lambda(|\phi|)$ as obtained by integration of the net particle balance of Fig.7. Particles move towards high $|\phi|$ as coherent structures grow. $\Lambda(|\phi|)$ is zero both for $|\phi| = 0$ and for high $|\phi|$, as the system neither gains nor loses particles. (b) The "flux" $M(|\phi|)$ of nonlinear energy. (c) The total flux of energy (nonlinear energy $M(|\phi|)$ plus coupling energy $\Pi(|\phi|)$) is negative, i.e. energy flows from high amplitudes to low amplitudes. (d) The "flux" of coupling energy $\Pi(|\phi|)$ is negative. The loss of coupling energy ΔE_2 in the flux $\Pi(|\phi|)$ is identical with the loss of coupling energy in the flux P in Fig.4. The loss of coupling energy ΔE_2 matches the gain ΔE_4 of nonlinear energy.

at $|\phi| \approx 1.8$. $\Pi(|\phi|)$ expresses in amplitude space the same loss of coupling energy as Fig.6(b) does for the flux $P(\omega)$ in frequency space. This loss of coupling energy ΔE_2 matches the gain of nonlinear energy ΔE_4 of Fig.8(b).

These gains and losses are caused by the external driving and damping, but the Hamiltonian dynamics reverses these changes. E_4 and E_2 each are not conserved under the Hamiltonian dynamics, which actually transforms nonlinear energy into coupling energy at the same rate as damping and driving feed in nonlinear energy, and dissipate coupling energy. As a consequence, E_4 and E_2 each have no gains or losses after an average cycle of driving, damping, and Hamiltonian evolution over one time unit. Nonlinear energy is produced mainly by the dissipation of particles at locations where the amplitude is high. The dissipation of coupling energy is also relevant for low-amplitude fluctuations. The total energy flux $M(|\phi|) + \Pi(|\phi|)$ (Fig.8(c)) is therefore directed from high amplitudes to low amplitudes. In wavenumber space, this is related to

the negative energy transfer $K(\omega)$ at high ω (Fig.6(b)). K is fed by the source of nonlinear energy, which is due to the dissipation at high frequencies. This energy is transformed into coupling energy in the window of transparency. $M(|\phi|)$, $\Pi(|\phi|)$ and $P(\omega)$ are not genuine fluxes, because E_2 and E_4 each are not conserved under the Hamiltonian dynamics. This causes the false impression of Figs.6(b),8(b),8(d) of permanent losses of E_2 and gains of E_4 . These quantities do not account for the k -nonlocal energy transformation of E_4 into E_2 . In contrast, $\Lambda(|\phi|)$ and $Q(\omega)$ as well as $M(|\phi|) + \Pi(|\phi|)$ are fluxes of the conserved quantities n and E respectively. In the weakly driven system (Fig.4(b)), $P(\omega)$ may also be considered as a flux, because E_2 is virtually constant under the Hamiltonian dynamics.

4.4 The energy cycle of collapses

We now investigate the Hamiltonian process that transforms energy E_4 into E_2 by studying the time-evolution, instead of averaged quantities. Figs.9,10 show a simulation with a medium-power driving force with $c = 13.6$. Fig.9(a) shows the maximum square amplitude $\max(|\phi|^2(x))$ that is reached at any location x in the system. The system has almost everywhere low amplitudes $|\phi|^2 < 0.3$, and high amplitude structures $|\phi|^2 > 1$ emerge only intermittently in small areas in space. The medium-power driving force allows us to distinguish different amplitude blow-ups in time, while a stronger driving force would lead to overlapping high-amplitude signals from simultaneous blow-ups at different locations. The fluxes of the cases $c = 13.6$ and $c = 27$ (Figs.6-8) have similar qualitative features. The weak driving force with $c = 2.4$ of Fig.4 leads to no such high-amplitude events, so that the maximum amplitude is of the order $|\phi|^2 \sim 0.01$.

It is not completely clear how these structures emerge from the random low-amplitude background. The nonlinear events are very similar to collapses in Hamiltonian partial differential equations such as the undamped MMT equation or the nonlinear Schrödinger equation. These can be described as heteroclinic orbits that connect the phase-unstable homogeneous mode with a localized structure with an infinite amplitude. A collapse contains a finite amount of particles with a zero energy, since its nonlinear energy is minus the coupling energy. Collapses may be regarded as a coherent and k -nonlocal mechanism that transports particles towards high wavenumbers [4], [17], [18]. Dissipation of short waves prevents the singularity, and leads to a decay of the peak.

In the focusing nonlinear Schrödinger equation, all plane waves are phase-unstable under slow modulations, but this mechanism is different in the MMT equation. A perturbation $\delta\phi = \exp(ikx)(a(t)\exp(ikx) + b(t)\exp(-ikx))$ of a plane wave $\phi = \sqrt{n}\exp(i(kx - (\omega - n)t))$ has an eigenvalue with a positive real part if $(2n - \nu)\nu > 0$ with $\nu = (\omega(k + q) + \omega(k - q) - 2\omega(k))/2$, which requires

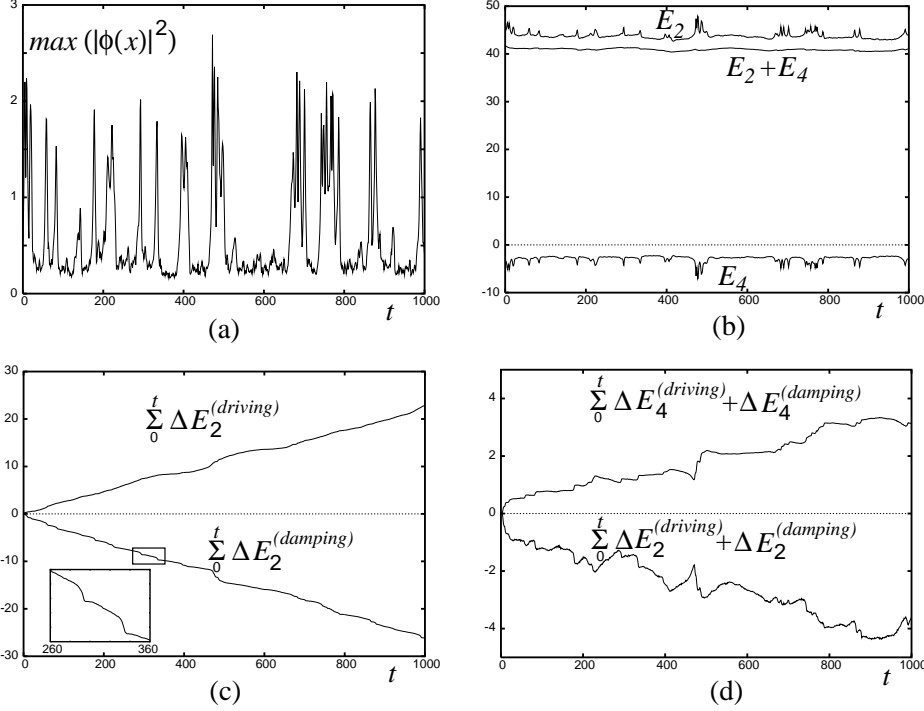


Fig. 9. Simulation with a medium-power driving force ($c = 13.6$). (a): Maximum of the squared amplitude $|\phi|^2$ that is reached anywhere in the system as a function of time. (b) E_2 , E_4 and $E_2 + E_4$ as functions of time. (c) Cumulated input of coupling energy by the driving force $\sum_0^t \Delta E_2^{(driving)}$, and cumulated output of coupling energy by the damping $\sum_0^t \Delta E_2^{(damping)}$. (d) Cumulated change of coupling energy by the damping and the driving force $\sum_0^t \Delta E_2^{(driving)} + \Delta E_2^{(damping)}$ (sum of the curves of (c)), and cumulated change of nonlinear energy by the damping and the driving force $\sum_0^t \Delta E_4^{(driving)} + \Delta E_4^{(damping)}$.

$0 < \nu < 2n$. For the focusing nonlinear Schrödinger equation, this is always fulfilled for small q since $\omega = k^2$ is convex and $\nu = q^2 > 0$. For the MMT equation, a necessary condition for an instability is that $k + q$ and $k - q$ have different signs, i.e. $|q| > |k|$. The homogeneous mode $k = 0$ is unstable under slow modulations, since the dispersion $\omega = \sqrt{|k|}$ is convex at this point. For waves with $k \neq 0$, the dispersion is concave, and an instability occurs only by interaction with remote modes, i.e. modes on both the left and the right branch of ω .

A possible starting point for collapses might be the built-up of a condensate at $k = 0$ by the inverse cascade [4]. The phase instability of the condensate might lead to a collapse as soon as enough particles have gathered at $k = 0$. However, in our simulations the low- k damping is so efficient that the homogeneous mode has a very low level. Collapses in our simulations occur while the homogeneous mode contains only $n_{k=0} \sim 0.1$ particles, i.e. the number of particles in the homogeneous mode of the whole system is below the particle number of a single collapse. In addition, we find no sign of a build-up of a

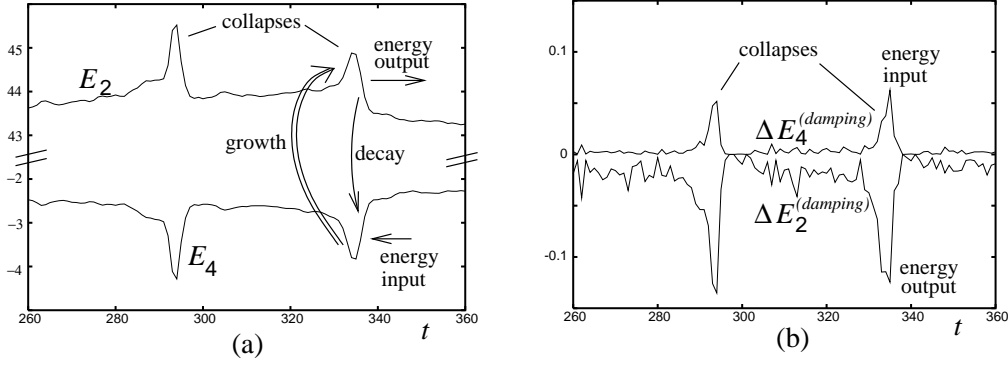


Fig. 10. (a): E_2 and E_4 as functions of time for the simulation of Fig.9. Energy is transferred from E_4 to E_2 during the growth of a peak. This energy is partly dissipated and partly transferred back to E_4 when the peak decays. The damping increases the energy E_4 . (b): Energy gain $\Delta E_4^{(damping)}$ and energy loss $\Delta E_2^{(damping)}$ by the damping.

condensate, as $n_{k=0}$ appears to be independent of the occurrence of collapses. Collapses occur in the same way for even more efficient low- k damping, where each damping step removes all particles with small wavenumbers. The collapse dynamics appears to depend crucially on the maximum power in the driving range, or equivalently, on the total particle number. Instabilities of waves in the driving range are strongly nonlocal in wavenumber space and cause no slow phase modulations.

Fig.9(b) shows the energies E_2 , E_4 , and $E = E_2 + E_4$ of the total system during the simulation. At each of the high-amplitude events, E_4 temporarily decreases, while E_2 increases by the same amount, and both energies approach their previous values subsequently. There is no net change of these energies on average.

Fig.9(c) shows the input and output of coupling energy as functions of time. $\sum_0^t \Delta E_2^{(driving)}$ is the input of coupling energy through the driving force cumulated over a period of time $[0, t]$, and $\sum_0^t \Delta E_2^{(damping)}$ is the corresponding output through the damping. Coupling energy is dissipated at an approximately constant rate between the collapses, which reflects a weakly turbulent transport of energy into the dissipation range between the collapses. The increased dissipation at times when high-amplitude structures emerge leads to step-like decays of $\sum_0^t \Delta E_2^{(damping)}$. The steps lead to an energy output that is bigger than the energy input from the driving, i.e. $\sum_0^t \Delta E_2^{(damping)} + \sum_0^t \Delta E_2^{(driving)} < 0$. This net output of coupling energy is shown in Fig.9(d) together with the net input of nonlinear energy $\sum_0^t \Delta E_4^{(damping)} + \sum_0^t \Delta E_4^{(driving)} > 0$. The time average of $\Delta E_2^{(damping)} + \Delta E_2^{(driving)}$ is just the energy-flux $P(\omega) = \Pi(|\phi|) = \Delta E_2$ at high ω or high $|\phi|$. The average of $\Delta E_4^{(damping)} + \Delta E_4^{(driving)}$ is the energy-flux $M(|\phi|) = \Delta E_4$ at high $|\phi|$. As there is no net change of the total energy, the gain of E_4 matches the loss of E_2 .

Fig.10 shows two of the collapses of the simulation of Fig.9. When a peak

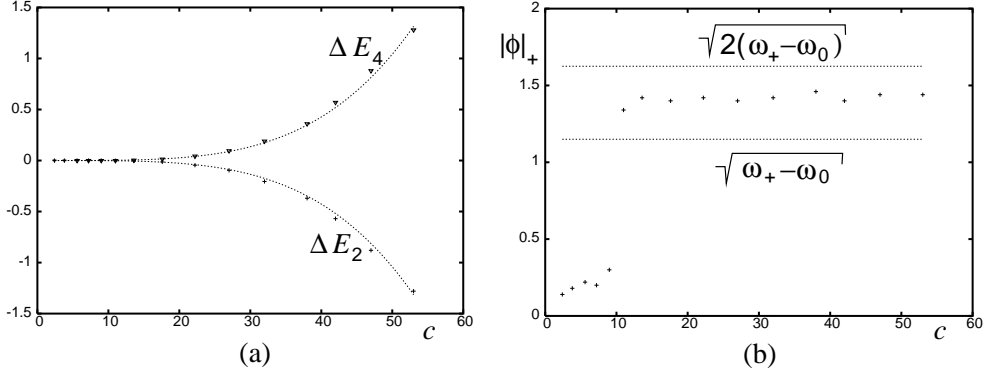


Fig. 11. (a) Net loss of coupling energy ΔE_2 and gain of nonlinear energy ΔE_4 versus the coefficient c of the power law $n_k = c/(kL/2\pi)$. ΔE_2 is the value of the energy flux P at high ω or Π at high $|\phi|$, ΔE_4 is the value of the flux of nonlinear energy M at high $|\phi|$. (b) Peak heights together with an upper and a lower estimate. The simulations are the same as in Fig.5.

emerges, the total coupling energy E_2 increases due to the high gradient of the peak. Simultaneously, the nonlinear energy E_4 decreases because of the locally high amplitude. The blow-up transfers energy from E_4 to E_2 .

The peak is strongly affected by the damping so that it loses coupling energy. Fig.10(b) shows this dissipation, where the spikes of the dissipation rate $\Delta E_2^{(damping)}$ correspond to the steps of $\sum_0^t \Delta E_2^{(damping)}$ of Fig.9(c). As the amplitude of the peak decreases by the action of the damping, the nonlinear energy increases again. Therefore the damping provides both an input of energy E_4 and an output of energy E_2 (Fig.10(b)). The picture of the energy cycle is that the damping feeds nonlinear energy ΔE_4 into the system, that is transformed to coupling energy ΔE_2 and subsequently dissipated. The burnouts of the peaks are incomplete [4], and some of the coupling energy is not dissipated, but returned to the nonlinear energy by a Hamiltonian process. Radiation of the decaying peak might also contribute to the low-amplitude waves.

Fig.11(a) shows the net output rate coupling energy ΔE_2 and the net input rate of nonlinear energy ΔE_4 that is caused by damping and driving. As in Fig.5, c measures the particle density that is obtained in the window of transparency for different driving powers. Again, we can distinguish between pure weak turbulence and collapses. For driving forces below the threshold $c \approx 10$, the cumulated dissipation of coupling energy (as in Fig.9(c)) has no steps, as there are no collapses. Average input and output of coupling energy are matching as $\Delta E_2^{(damping)} + \Delta E_2^{(driving)} = \Delta E_2 \approx 0$, and the input of nonlinear energy $\Delta E_4^{(damping)} \approx 0$ and $\Delta E_4^{(driving)} \approx 0$ is negligible. Above the threshold, output of coupling energy and input of nonlinear energy by damping and driving match closely as $\Delta E_2 = -\Delta E_4$. The lines give a tentative fit $\sim c^4$.

A characteristic peak height can be defined as the amplitude where the nonlinear energy change by the damping and driving is maximal, i.e. $|\phi|$ of Fig.7 with the maximum $|\Delta E_{4|\phi}|$. Fig.11(b) shows this peak height $|\phi|_+$ versus the coefficient c of the power spectrum. Again, high amplitudes appear only for

strong driving forces. Below the threshold, $|\Delta E_{4|\phi}|$ is very small and negligible in the energy balance. To give an estimate the height of these structures, we assume that Δn particles carrying an energy $\omega_0 \Delta n$ are injected at ω_0 , and they are removed at ω_+ where they carry the coupling energy $\omega_+ \Delta n$. The net energy loss $\Delta E_2 = (\omega_0 - \omega_+) \Delta n$ from this process can be balanced by a gain of nonlinear energy due to a particle flow towards high amplitudes where the particles are dissipated. If we assume for simplicity that the damping reduces the amplitude $|\phi|$ by $\Delta|\phi| \ll |\phi|$ in the interval Δx in space, an amount of $\Delta n = 2|\phi|\Delta|\phi|\Delta x$ particles are removed and the nonlinear energy is increased by $\Delta E_4 = |\phi|^2 \Delta n$. With the energy balance $\Delta E_4 + \Delta E_2 = 0$, we obtain $|\phi| = \sqrt{\omega_+ - \omega_0}$ as a lower estimate for the height of the peaks. For an upper estimate, we assume that the damping decreases the amplitude by $\Delta|\phi| = |\phi|$ and removes all particles $\Delta n = |\phi|^2 \Delta x$ from this interval, so that the gain of nonlinear energy is $\Delta E_4 = |\phi|^4 \Delta x / 2 = |\phi|^2 \Delta n / 2$. For this case, the energy balance gives $|\phi| = \sqrt{2(\omega_+ - \omega_0)}$ as an upper estimate of the peak height. If the particles input by the driving force has an average $\omega_0 \approx 0.2$ and the particle output occurs at $\omega_+ \approx 1.5$, we expect a peak height between $|\phi| \approx 1.1$ and $|\phi| \approx 1.6$, compared to the numerical result $|\phi| \approx 1.4$.

5 Conclusions

We have studied the fluxes of energy and particles in a onedimensional turbulent system, the focusing Majda-McLaughlin-Tabak equation. These fluxes reveal details about the statistically stationary state that cannot be observed directly in the conserved quantities, such as the spectrum of particles n_k (Fig.2). Fluxes in frequency space (Figs.4,6) have sources and sinks that are determined by the external driving and damping. Fluxes in amplitude space (Fig.8) emerge spontaneously when the total particle input rate exceeds a threshold (Fig.5).

We have found two types of nonequilibria with similar spectra (Fig.2(a)), but very different energy fluxes. The nonequilibrium state for sufficiently weak driving is very similar to the weakly turbulent Zakharov solution. The average amplitude is small, with an exponentially decreasing probability for higher amplitudes (Fig.2(b)). Nonlinearity only plays a role as a weak coupling between the dispersive waves, and no high-amplitude structures emerge. Particles that are injected at the driving scale flow toward the sinks both at high and at low wavenumbers (Fig.4(a)). We interpret the well-known quantities [1] $Q\omega$ and K (Fig.4(b)) as energy drift and energy transfer. In particular, K transfers energy that is released in the inverse cascade to the direct cascade, where it is absorbed. The fluxes increase slightly faster with the particle density (Fig.5(a)) than predicted by the theory of weak turbulence.

For stronger driving forces, high amplitude structures emerge intermittently,

and the interaction becomes strongly nonlinear. The energy balance changes in two ways: Firstly, more coupling energy is dissipated by the damping than supplied by the driving force. This leads to a negative energy flux P and energy transfer K for high frequencies (Fig.6(b)). Secondly, damping and driving provide a net surplus of nonlinear energy E_4 , which is due to the dissipation of particles at high amplitudes (Figs.7,8(b)). This is related to fluxes of particles and energy in amplitude space (Fig.8). There is a net particle flux from low amplitudes, where the driving force injects particles, toward high amplitudes, where particles are removed by the dissipation (Fig.8(a)). The dissipation of particles at the tip of high-amplitude structures is the source of an energy flux from high amplitudes to low amplitudes, where coupling energy is dissipated (Fig.8(c)).

While driving and damping cause a permanent net input of E_4 and an equal net output of E_2 , both the coupling energy and the nonlinear energy are constant with only small fluctuations (Fig.9(b)). This is possible because the Hamiltonian dynamics transforms nonlinear energy into coupling energy within the energy flux from high to low amplitudes (Fig.8(c)). This transformation of nonlinear energy into coupling energy occurs during the blow-ups (Figs.9,10), where the coupling energy increases and the nonlinear energy decreases. Coupling energy can be radiated into the surrounding low-amplitude waves, when, for example, a peak emerges out of two colliding solitary waves [21]. A peak that decays after reaching its maximum height can also radiate low-amplitude waves. The generation of coupling energy at high ω feeds the energy transfer K , that is directed toward low frequencies at high ω . The representation of energy fluxes in frequency or wavenumber space is somehow misleading since it neglects the k -nonlocal transformation nonlinear energy into coupling energy.

The nonlinear energy E_4 is related to high-amplitude coherent structures, while the coupling energy E_2 has contributions both from these peaks and from low-amplitude fluctuations. The advantage of studying these two quantities (and not peaks and fluctuations) is that their fluxes are measurable statistical quantities that distinguish weakly turbulent and coherent processes. The fluxes in wavenumber or frequency space and in amplitude space may be seen as two projections of the complex highdimensional transport process. In wavenumber space, driving and damping is related to localized sources and sinks of the fluxes. The fluxes yield the boundary conditions for the nonequilibrium in the inertial range. This is appropriate for the pure weakly turbulent process, where the statistics is almost Gaussian and higher order correlations can be reduced to two-point functions. If the statistics is non-Gaussian, the external forces inject energy to the nonlinear part of the Hamiltonian E_4 (i.e. the four-point correlation) and remove energy from E_2 , the two-point correlation. The Hamiltonian dynamics is characterized by the transformation of energy E_4 into E_2 , which is actually the transfer of a conserved quantity between correlations of different order. The representation in amplitude space covers this spontaneous coherent process, which appears as an energy flux from high

amplitudes to low amplitudes. The representations in wavenumber space and in amplitude space together cover the energetics of this process. The many open questions on the energy transfer from E_4 to E_2 concern, in particular, the onset of this coherent behavior. Also, the effect of the coherent structures on the low-amplitude process by radiation is not well understood.

References

- [1] V.E.Zakharov, V.Lvov, G.Falkovich, Kolmogorov spectra of turbulence, Springer-Verlag, Berlin, 1992
- [2] L.Biven, S.V.Nazarenko, A.C.Newell, Phys.Lett.A 280 (2001) 28-32
A.C.Newell, S.V.Nazarenko, L.Biven, Physica D 152-153 (2001) 520-550
- [3] N.E.Kosmatov, V.F.Shvets, and V.E.Zakharov, Physica D 52 (1991) 16-35
- [4] S.Dyachenko, A.C.Newell, A.Pushkarev, V.E. Zakharov, Physica D 57 (1992) 96-160
- [5] B.Rumpf and A.C.Newell, Phys. Rev. Lett. 87 (2001) 054102
B.Rumpf and A.C.Newell, Physica D 184 (2003) 162
- [6] S.L.Musher, A.M.Rubenchik, V.E.Zakharov, Phys.Rep.252 (1995) 177-274
- [7] E.Henry, P.Alstrom, M.T.Levinsen, Europhys.Lett.52 (2000) 27-32
- [8] A.I.Dyachenko, A.O. Korotkevich, V.E.Zakharov, Phys.Rev.Lett.92 (2004) 134501
Y.V.Lvov, E.G.Tabak, Phys.Rev.Lett.87 (2001) 168501
- [9] S.Galtier, S.V.Nazarenko, A.C.Newell, A Pouquet, J.Plasma Phys. 63 (2000) 447-488
S.Galtier, S.V.Nazarenko, A.C.Newell, Physica D 152-153 (2001) 646-652
- [10] Y.Lvov, S.Nazarenko, R.West, Physica D 184 (2003) 333-351
C.Josserand, C.R.Physique 5 (2004) 77-90
- [11] V.E.Zakharov, Zh.Eksp.Teor.Fiz.62 (1972) 1745-1759 (Sov.Phys.JETP 35 (1972) 908-914)
- [12] P.L.Kelley, Phys.Rev.Lett.15 (1965) 1005-1008
E.Garmire, R.Y.Chiao, C.H.Townes, Phys.Rev.Lett.16 (1966) 347-349,
V.E.Zakharov, V.V.Sobolev, V.C.Synakh, Zh.Eks.Teor.Fiz.60 (1971) 136-145
(Sov.Phys.JETP 33 (1971) 77-81)
- [13] P.G.Saffman, J.Fluid Mech.27 (1967) 581-593
- [14] B.Rumpf and A.C.Newell, Phy. Rev.E 69 (2004) 026306
- [15] A.J.Majda, D.W.McLaughlin, E.G.Tabak, J.Nonlinear Sci. 6, (1997) 9-44

- [16] D.Cai, D.W.McLaughlin, *Physica D* 152-153 (2001) 551-572
J.Math.Phys.41 (2000) 4125-4153 D.Cai, A.J.Majda, D.W.McLaughlin,
E.G.Tabak, PNAS 96 (1999) 14216-14221
- [17] V.E.Zakharov, P.Guyenne, A.N.Pushkarev, F.Dias, *Physica D* 152-153 (2001)
573-619
- [18] V.Zakharov, F. Dias, A. Pushkarev, *Physics Reports* 398 (2004) 1-65
- [19] J.Spanier, K.B.Oldham, *The Fractional calculus: Integrations and
Differentiations of Arbitrary Order*, Academic Press, New York (1974)
- [20] B.Rumpf, *Phys. Rev. E* 69 (2004) 016618
B.Rumpf, *Phys. Rev. E* 70 (2004) 016609
- [21] S.Dyachenko, V.E.Zakharov, A.N.Pushkarev, V.F.Shvets, V.V.Yankov, *Zh.
Eksp. Teor. Fiz.*96 (1989) 2026-2032 (*Sov. Phys. JETP* 69 (1989) 1144-1147)